Available online at www.sciencedirect.com
ScienceDirect
Journal of Sound and Vibration 323 (2009) 1003–1015
JOURNAL OF SOUND AND VIBRATION
www.elsevier.com/locate/jsvi

Steady-state response of a cantilever plate subjected to harmonic displacement excitation at the base

D.J. Gorman[a,*], R. Singhal[b]

[a]*Department of Mechanical Engineering, The University of Ottawa, Ottawa, Canada*
[b]*Structural Qualification Facilities, David Florida Laboratory, CSA, Ottawa, Canada*

Received 16 April 2008; received in revised form 9 January 2009; accepted 13 January 2009
Handling Editor: C.L. Morfey
Available online 14 February 2009

Abstract

An interest in the dynamic steady-state response of cantilever plates to harmonic lateral and rotational displacement imposed along the clamped edge has arisen in connection with the projecting of lifetimes of electronic components mounted on the plate lateral surface. Analytical type solutions to the problem are obtained by exploiting the superposition method, a method which has previously been successfully exploited to obtain accurate solutions for free vibration problems involving rectangular plates with various combinations of boundary conditions, point supports, etc. This newly developed approach to free vibration problem analysis has been modified here to handle forced vibration problems, in particular, to calculate response of cantilever plates of two different geometries to a range of base excitation frequencies. The theoretical work has been supported by a careful parallel experimental program. Very good agreement between theory and experiment has been encountered. It is expected that the theoretical approach described will provide a powerful analytical means for obtaining accurate solutions to various other rectangular plate forced vibration problems.

1. Introduction

In this paper analytical type solutions are obtained for the steady-state response of undamped cantilever plates subjected to lateral and torsional harmonic excitation along the clamped edge. The theoretical work is accompanied by an experimental program which provides valuable test data for verification of the computational procedure. The computational procedure itself is based on the method of superposition. This method has been widely exploited to obtain accurate analytical type solutions for plate free lateral vibration problems. See for example Ref. [1]. The present paper demonstrates for the first time how this same method can be employed to solve rectangular plate steady-state forced vibration problems.

A fairly good discussion on the mathematical procedures employed heretofore to solve forced plate transverse vibration problems is to be found in the work of Szilard [2]. He also provides a relevant list of references. Analysis of forced vibration problems differ from those of free vibration (as will be seen) in that the

*Corresponding author. Tel.: +1 613 562 5800x6279; fax: +1 613 562 5177.
E-mail address: dgorman@genie.uottawa.ca (D.J. Gorman).

0022-460X/$ - see front matter © 2009 Elsevier Ltd. All rights reserved.
doi:10.1016/j.jsv.2009.01.020

Nomenclature

a, b	rectangular plate edge dimensions
D	plate flexural rigidity, equals $Eh^3/12(1-v^2)$
E	Young's modulus of plate material
h	plate thickness
K	number of terms used in solution series
V	plate vertical edge reaction
V_η	dimensionless vertical edge reaction along edges parallel to ξ-axis $= V\phi b^2/D$
V_ξ	dimensionless vertical edge reaction along edges parallel to η-axis $= Va^2/D$
W	plate lateral displacement divided by edge length "a".
x, y	distances along plate coordinate axes
ξ, η	dimensionless distances along plate coordinate axes, $\xi = x/a$, $\eta = y/b$
λ^2	dimensionless frequency of plate vibration, $\lambda^2 = \omega a^2\sqrt{\rho/D}$
λ_f^2	dimensionless frequency of plate edge excitation, $\lambda_f^2 = \omega_f a^2\sqrt{\rho/D}$
ρ	mass of plate per unit area
v	Poisson ratio of plate material
v^*	$=2-v$
ϕ	plate aspect ratio equals b/a
ω	radian frequency of plate vibration
ω_f	radian frequency of harmonic excitation imposed on plate driven edge

governing differential equation(s) are no longer homogeneous. As a result, particular solutions as well as homogeneous solutions must be obtained for the equation system. So long as one restricts oneself to rectangular plates with simple support on all edges the problems are greatly simplified and Navier type solutions can usually be obtained [2]. It is pointed out by Szilard that beyond the above limited class of problems analytical type solutions are usually difficult, if not impossible, to obtain. It is natural in such cases to seek solutions by resorting to energy techniques. Also, with the advent of high speed digital computers and finite element methods one can turn to numerical solutions.

The superposition method as applied here has the advantage that it can be employed to obtain accurate converging solutions regardless of the combination of classical boundary conditions specified. One should also recognize that solutions obtained by this method satisfy exactly the governing equation(s) throughout the entire domain of the plate. Boundary conditions are satisfied to any desired degree of accuracy by increasing the number of terms utilized in the solution.

An interest in the present problem has arisen in connection with design concerns related to the electronics industry (Electronic Packaging). It is well known that highly accurate analytical type solutions have been obtained for free vibration frequencies and mode shapes of cantilever plates by exploitation of the method of superposition [3,4]. Here, it is shown how the same method can be extended to the domain of forced vibration problems and, in particular, to the obtaining of forced vibration steady-state response of the base-driven cantilever plate.

2. Mathematical procedure

In the earlier publications referred to above, the two free vibration mode families characteristic of cantilever plates, those symmetric and those anti-symmetric about the plate centre line running perpendicular to the plate clamped edge, were treated separately. The advantages of this approach were discussed. It is found that in obtaining solutions to the general forced vibration problem addressed here, such a mode family delineation is not usually applicable. In fact, it is found advantageous to begin the problem undertaken here by setting up the general system of equations required to perform a general free vibration analysis of the entire plate. Later it will be shown how this system of equations is modified in order to resolve the forced vibration problem of interest.

2.1. The general free vibration analysis

A general free vibration analysis of the cantilever plate is achieved here by the superposition method. In this method, following established procedures, a judiciously selected set of forced vibration problem solutions (building blocks), which satisfy exactly the governing differential equation, are superimposed,

one-upon-the-other, and driving coefficients appearing in these building block solutions are constrained in such a way that the net solution thereby obtained satisfies, not only the governing differential equation, but prescribed boundary conditions to any desired degree of accuracy. Some readers may wish to consult Refs. [3,4] in order to familiarize themselves with procedures followed.

We begin by superimposing the four building blocks shown schematically in Fig. 1. Pairs of small circles adjacent to an edge indicate that slip–shear conditions are imposed along this boundary, i.e., the edge is free of vertical edge reaction and slope taken normal to the edge is everywhere zero. The first, second, and third building blocks are driven by a distributed harmonic edge rotation imposed along the driven edges and indicated by small circular arrows. Vertical edge reaction along these driven edges is everywhere zero. The fourth building block is driven by a distributed vertical edge reaction indicated by small straight arrows. Slope taken normal to this driven edge is forbidden, a condition indicated by a pair of very small circles adjacent to the arrows.

We begin by examining the first building block. Slip–shear support is imposed along the edge, $\xi = 0$. The governing differential equation is written in dimensionless form as [4]

$$\frac{\partial^4 W(\xi,\eta)}{\partial\eta^4} + 2\phi^2 \frac{\partial^4 W(\xi,\eta)}{\partial\eta^2\partial\xi^2} + \phi^4 \frac{\partial^4 W(\xi,\eta)}{\partial\xi^4} - \phi^4\lambda^4 W(\xi,\eta) = 0. \tag{1}$$

Solution for this building block is taken in the form proposed by Levy as

$$W(\xi,\eta) = \sum_{m=1,2}^{K} Y_m(\eta)\cos\, emp\,\xi, \tag{2}$$

where we introduce the symbols $emp = (m-1)\pi$ and $emps = emp$ squared. It is noted that each term of the series satisfies exactly the slip–shear boundary conditions imposed along the edges, $\xi = 0$ and 1.

Substituting Eq. (2) into Eq. (1) it is found that the variables are separable and we obtain a fourth-order ordinary homogeneous differential equation governing the quantities $Y_m(\eta)$. Solutions to this equation are well known and are found in Eqs. (3) and (4). The constants of integration, A_m, B_m, etc., are evaluated through enforcement of prescribed boundary conditions.

For $\lambda^2 > emps$

$$Y_m(\eta) = A_m \cosh\,\beta_m\eta + B_m \sinh\,\beta_m\eta + C_m \cos\,\gamma_m\eta + D_m \sin\,\gamma_m\eta \tag{3}$$

and, for $\lambda^2 < emps$

$$Y_m(\eta) = A_m \cosh\,\beta_m\eta + B_m \sinh\,\beta_m\eta + C_m \cosh\,\gamma_m\eta + D_m \sinh\,\gamma_m\eta, \tag{4}$$

where

$$\beta_m^2 = \phi^2[\lambda^2 + emps] \quad \text{and} \quad \gamma_m^2 = \phi^2[\lambda^2 - emps] \text{ or } \phi^2[emps - \lambda^2]$$

whichever is positive.

It will be observed that, in view of the slip–shear conditions to be enforced along the edge, $\eta = 0$, B_m and D_m must equal zero.

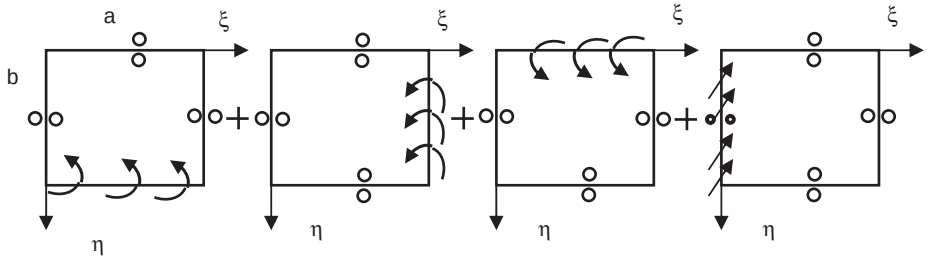

Fig. 1. Schematic representation of building blocks employed in solving free vibration problem.

Vertical edge reaction along the edge, $\eta = 1$, is expressed in dimensionless form as [4]

$$V_\eta = -\left\{\frac{\partial^3 W(\xi,\eta)}{\partial\eta^3} + \upsilon^*\phi^2\frac{\partial^3 W(\xi,\eta)}{\partial\eta\partial\xi^2}\right\}. \tag{5}$$

Focusing attention on the first form of solution (Eq. (3)) and enforcing the condition of zero vertical edge reaction along the driven edge it is readily shown that we may write for any value of m,

$$Y_m(\eta) = A_m[\cosh\,\beta_m\eta + \theta_{1m}\cos\,\gamma_m\eta], \tag{6}$$

where

$$\theta_{1m} = -\frac{\beta_m[\beta_m^2 - \upsilon^*\phi^2\,emps]\sinh\,\beta_m}{\gamma_m[\gamma_m^2 + \upsilon^*\phi^2\,emps]\sin\,\gamma_m}.$$

We next consider the amplitude of the harmonic edge rotation imposed along the driven edge to be expanded in a cosine series as employed in Eq. (2), i.e.,

$$\left.\frac{\partial W(\xi,\eta)}{\partial\eta}\right|_{\eta=1} = \sum_{m=1,2}^{K} E_m\cos\,emp\,\xi, \tag{7}$$

where the quantity E_m represents the driving coefficients. Enforcing the equality of Eq. (7), for any value of m, it is readily shown that we may write

$$Y_m(\eta) = E_m\theta_{11m}[\cosh\,\beta_m\eta + \theta_{1m}\cos\,\gamma_m\eta], \tag{8}$$

where

$$\theta_{11m} = \frac{1}{(\beta_m\sinh\,\beta_m - \theta_{1m}\gamma_m\sin\,\gamma_m)}.$$

We next turn to the second form of the solution, Eq. (4). Following steps identical to those described above it is shown that

For $\lambda^2 \leqslant emps$

$$Y_m(\eta) = E_m\theta_{22m},[\cosh\,\beta_m\eta + \theta_{2m}\cosh\,\gamma_m\eta], \tag{9}$$

where

$$\theta_{2m} = -\frac{\beta_m}{\gamma_m}\frac{(\beta_m^2 - \upsilon^*\phi^2\,emps)}{(\gamma_m^2 - \upsilon^*\phi^2\,emps)}\frac{\sinh\,\beta_m}{\sinh\,\gamma_m}$$

and

$$\theta_{22m} = \frac{1}{(\beta_m\sinh\,\beta_m + \theta_{2m}\gamma_m\sinh\,\gamma_m)}.$$

We thus have available the solution for response of the first building block to any harmonic rotation imposed along the driven edge.

A solution for response of the second building block, also driven by a distributed harmonic edge rotation, is easily extracted from that of the first. Here, we will utilize the subscript n in order to avoid confusion with the first building block solution. The solution will take the form

$$W(\xi,\eta) = \sum_{n=1,2}^{K} Y_n(\xi)\cos\,enp\,\eta, \tag{10}$$

where $enp = (n-1)\pi$. The driving rotation amplitude is expressed as

$$\frac{\partial W(\xi,\eta)}{\partial\xi} = \sum_{n=1,2}^{K} E_n\cos\,enp\,\eta. \tag{11}$$

Before extracting the solution for $Y_n(\xi)$ we must introduce certain temporary changes as follows. First replace λ^2 with $\lambda^2\phi^2$. Next, temporarily replace ϕ with $1/\phi$. Solution for the quantities $Y_n(\xi)$ are obtained from the earlier quantities $Y_m(\eta)$ by replacing η with ξ. Quantities θ_{1n}, θ_{11n} etc., are extracted from the quantities θ_{1m}, θ_{11m}, etc., by replacing β_m and γ_m with their counterparts β_n and γ_n (Eq. (4)), also replace *emps* with *enps* where $enps = ((n-1)\pi)^2$.

We thus have available solution for response of the second building block to any harmonic rotation imposed along the driven edge.

Solution for response of the third building block will differ from that of the first, only in that the quantity η of the first solution should now be replaced by the quantity $(1-\eta)$. Terms of this new solution should be preceded by a negative sign in view of our sign conventions.

We turn finally to the fourth building block of Fig. 1. It is found advantageous to begin by solving for response of the building block shown schematically in Fig. 2(a).

The solution is taken in the form

$$W(\xi,\eta) = \sum_{m=1,2}^{K} Y_m(\eta)\cos(m-1)\pi\xi. \tag{12}$$

A condition of zero slope is imposed along the edge, $\eta = 1$. This edge is driven by a distributed harmonic vertical edge reaction as indicated in the figure. Solutions for the function $Y_m(\eta)$ will have a form identical to those of the first building block, however, here different boundary conditions are imposed along the driven edge. Enforcing the condition of zero slope along the driven edge it is readily shown that for the first form of solution we may write

$$Y_m(\eta) = A_m[\cosh\ \beta_m\eta + \theta^{|}_{1m}\cos\ \gamma_m\eta], \tag{13}$$

where

$$\theta^{|}_{1m} = \frac{\beta_m\ \sinh\ \beta_m}{\gamma_m\ \sin\ \gamma_m}.$$

The superscript prime is introduced here to avoid confusion with the first building block. The distributed amplitude of the vertical edge reaction driving the building block is expressed as

$$V_\eta(\xi) = \sum_{m=1,2}^{K} E^{|}_m\ \cos(m-1)\pi\xi. \tag{14}$$

Enforcing this edge condition, following a procedure similar to that described for the first building block, we obtain

For $\lambda^2 > emps$

$$Y_m(\eta) = E^{|}_m\theta^{|}_{11m}[\cosh\ \beta_m\eta + \theta^{|}_{1m}\cos\ \gamma_m\eta], \tag{15}$$

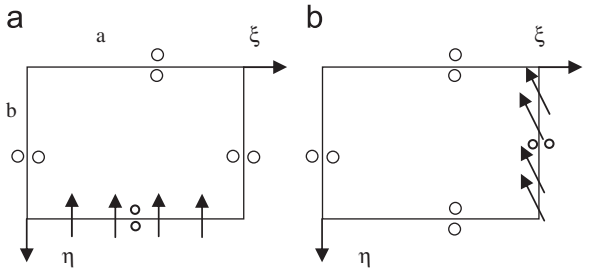

Fig. 2. Schematic representation of intermediate building block configurations: (a) driven along edge, $\eta = 1$ and (b) driven along the edge, $\xi = 1$.

where

$$\theta^{|}_{11m} = \frac{-1}{\beta_m(\beta_m^2 - v^*\phi^2\, emps)\sinh\,\beta_m + \theta^{|}_{1m}\gamma_m(\gamma_m^2 + v^*\phi^2\, emps)\sin\,\gamma_m}.$$

Following analogous steps for the case where $\lambda^2 < emps$, one obtains

$$Y_m(\eta) = E^{|}_m\theta^{|}_{22m}[\cosh\,\beta_m\eta + \theta^{|}_{2m}\cosh\,\gamma_m\eta], \tag{16}$$

where

$$\theta^{|}_{2m} = -\frac{\beta_m\sinh\,\beta_m}{\gamma_m\sinh\,\gamma_m}$$

and

$$\theta^{|}_{22m} = \frac{-1}{\beta_m(\beta_m^2 - v^*\phi^2\, emps)\sinh\,\beta_m + \theta^{|}_{2m}\gamma_m(\gamma_m^2 - v^*\phi^2\, emps)\sinh\,\gamma_m}.$$

Solution for the building block of Fig. 2(b) is extracted from the above solution in a manner identical to that employed in extracting solution for the second building block of Fig. 1 from that of the first. Finally, solution for the fourth building block of Fig. 1 is obtained by replacing the parameter η of this latest solution (Fig. 2(b)) with the quantity $1-\eta$ and preceding it with a negative sign.

Solutions for each of the building blocks of Fig. 1 are therefore now available.

2.2. Generation of free vibration eigenvalue matrix

The free vibration eigenvalue matrix associated with the set of building blocks of Fig. 1 is generated following well-established procedures. The first set of homogeneous algebraic equations relating the driving coefficients E_m, E_n, etc., is obtained by requiring the net contribution of the four building blocks to bending moment along the edge, $\eta = 1$, to vanish. To achieve this we expand the net contribution in an appropriate trigonometric series. We then impose the condition that each term in this new boundary series should vanish. It is appropriate to utilize the cosine series of Eq. (2) for this expansion. This gives rise to a set of K homogeneous algebraic equations relating the $4K$ driving coefficients.

In a similar manner we require that net moment along the edges, $\xi = 1$ and $\eta = 0$, should vanish. This gives rise to two additional sets of K homogeneous algebraic equations relating the driving coefficients. Finally, we impose in a similar fashion, the condition that net displacement along the edge, $\xi = 0$, must vanish. We thus obtain a combined set of $4K$ homogeneous algebraic equations relating the $4K$ driving coefficients. The coefficient matrix of this combined set constitutes our eigenvalue matrix. Free vibration eigenvalues are those values of the dimensionless frequency, λ^2, which cause the determinant of this matrix to vanish.

A schematic representation of the eigenvalue matrix is provided in Fig. 3. Subscripts p and q are introduced to indicate driving coefficients related to the third and fourth building blocks, respectively. Non-zero elements of the matrix are indicated by short horizontal bars. Small figures inserted above the matrix segments indicate the building blocks to which these segments pertain. Other small figures to the right of rows of matrix segments indicate the plate edge along which boundary conditions are being enforced.

2.3. Plate forced vibration study

We now consider modifications to the above matrix which will permit computation of plate response to forced lateral rigid body harmonic translational or torsional motion imposed at the base. This requires the constructing of a set of non-homogeneous algebraic equations. The coefficient matrix of this non-homogeneous set is comprised of the first $4K$ rows and columns of the matrix of Fig. 3. The right-hand-side of this non-homogeneous set of equations comprises $4K$ elements. All of the first $3K$ elements of this column are set equal to zero. The remaining elements of the column depend on the type of displacement excitation to which the plate is subjected.

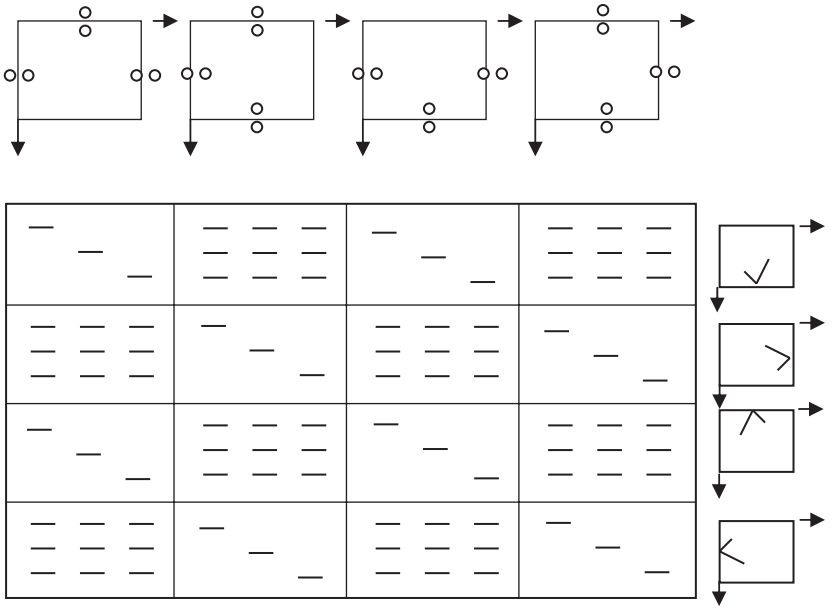

Fig. 3. Schematic representation of eigenvalue matrix based on three-term solution series.

Consider first, for illustrative purposes, the case where we wish to subject the base to a uniform lateral harmonic translation excitation of dimensionless amplitude equal to unity. We expand the amplitude of the translation in a cosine series of the form

$$W(\xi,\eta)_{|\xi=0}=\sum_{m=1}^{K}A_m\cos(m-1)\pi\eta. \tag{17}$$

It will be obvious, in view of the choice for dimensionless amplitude of base translation, that we will have, $A_m=1$, for $m=1$, with all other expansion coefficients equal zero. Accordingly, only one element of the column on the right hand side of the above set of non-homogeneous equations will be non-zero, that is the element $3K+1$ from the top, which equals unity. It follows that having chosen a value for ω_f, the driving radian frequency, and hence a value for λ_f^2, the dimensionless driving frequency, the steady-state response of the driven plate is easily obtained by solving the above set of non-homogeneous equations. All boundary conditions are satisfied to any desired degree of accuracy by simply increasing, K, the number of terms utilized in the building block series solutions.

Before examining computed results it is appropriate to examine the same problem where base excitation of the torsional or rocking type is employed. We will consider dimensionless amplitude of the base excitation to vary linearly from $+1$ to -1, as we move along the η-axis located at the base of the plate. Amplitude of the imposed harmonic displacement is expressed as,

$$W(\xi,\eta)_{|\xi=0}=1-2\eta. \tag{18}$$

Returning to the series of Eq. (17), it is easily shown that for each term m, with $m\gg1$, we have

$$A_m=2\left\{\frac{\sin(m-1)\pi}{(m-1)\pi}-2\left[\frac{\cos(m-1)\pi-1}{((m-1)\pi)^2}+\frac{\sin(m-1)\pi}{(m-1)\pi}\right]\right\} \tag{19}$$

while with $m=1$, the quantity A_m will equal zero. It will be appreciated that the dimensionless amplitude of any imposed lateral or rocking motion may be set at any desired level by simply multiplying the above coefficients, A_m, by an appropriate scalar quantity.

Upon entering these quantities in the coefficient matrix, response of the plate to any linearly distributed torsional motion of any driving frequency imposed at the base is readily computed.

3. Experimental apparatus and test procedures

In parallel with the theoretical studies reported here an experimental test program was carried out. This involved an experimental study of the steady-state response of two different cantilever plates subjected to uniform lateral harmonic excitation at the clamped edge. Both plates were fabricated from T6061 aluminium sheet. One plate was square, having dimensions 12×12 in (30.48×30.48 cm) with a thickness of 0.0625 in (0.1588 cm). The other plate was rectangular having dimensions 12×15 in (30.48×38.10 cm) and the same thickness. Each plate was clamped along a 12 in edge while conducting tests. The plates were mounted on an MB C-150 shaker by means of a specially prepared fixture. A view of the square plate mounted on the shaker expander head is shown in Fig. 4. Two accelerometers, one for excitation input control and one for response measurement were mounted as shown in the same figure. The response measuring accelerometer (Endevco Model 2222C, 0.5 g) was mounted at the mid point along the 12 in plate edge opposite the driven edge. In order to identify plate resonant frequencies, a low level (0.25 g constant acceleration input) sine sweep at the sweep rate of 1.0 octaves/min was performed on each plate for the frequency bandwidth of 5–500 Hz. In measuring the steady-state response of each plate at different excitation frequencies, the peak-to-peak input displacement excitation level was maintained constant at a peak-to-peak value of 0.125 in (0.3176 cm) for all frequencies. In order to measure steady-state response precisely, sine dwells were performed on each plate with 0.01 Hz resolution and a slow sweep rate of 1.0 Hz/min.

4. Presentation of theoretical and experimental results

It is pointed out that for all computations reported here a value of 15 is assigned to the parameter K, the number of terms employed in the building block series solutions. It is found that higher values assigned to K do not lead to any significant changes in the first four significant digits of computed eigenvalues or plate response calculations. Results of a convergence study related to computation of first mode eigenvalue for a square cantilever plate are tabulated in Table 1.

The first computational step was to verify that the general analytical model described here computes eigenvalues for the cantilever plate in good agreement with the well-known eigenvalues for this plate found in the literature. Eigenvalues for symmetric and anti-symmetric free vibration modes of the cantilever plate, as described earlier, are to be found in Refs. [3,4], for example. One may also wish to consult Ref. [5]. It is sufficient to say here that comparisons made between numerous eigenvalues listed in the earlier publications and corresponding eigenvalues computed by means of the general computational scheme described here are found to be in good agreement, often up to four significant digits. Eigenvalues computed by the present analytical scheme are compared with earlier published data for the first four free vibration modes of a square

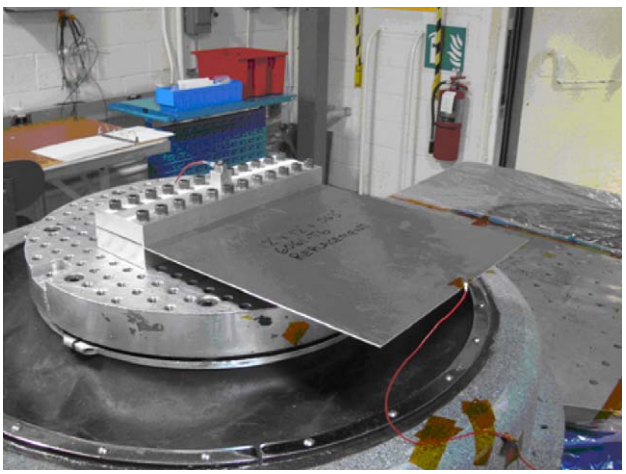

Fig. 4. Photograph of shaker table with square aluminium plate mounted in test position.

Table 1
Eigenvalue λ^2 vs. number of terms K employed, in convergence study related to computation of first mode free vibration of square cantilever plate.

K	7	9	11	13	15	17
λ^2	3.453	3.456	3.457	3.458	3.458	3.458

Table 2
Comparison of computed eigenvalues for square cantilever plate.

Mode	($v = 0.333$)		($v = 0.3$)	
	Pres.	Ref. [4]	Pres.	Ref. [5]
(1)	3.458	3.459	3.470	3.492
(2)	8.352	8.356	8.503	8.525
(3)	21.08	21.09	21.28	21.43
(4)	27.06	27.06	27.20	27.33

cantilever plate in Table 2. This comparison serves to provide a high level of confidence in the present computational scheme. It will be noted that eigenvalues of Ref. [5] are slightly higher than those computed by the present scheme. It is pointed out that the earlier eigenvalues were computed by employing the Ritz method. It is agreed that this latter method always provides upper limits for the eigenvalues. Actual eigenvalues will be equal to, or lower than these limits. It is therefore not surprising that results obtained by the present method are somewhat lower.

We turn therefore to comparing theoretical and experimental results for response of the base driven cantilever plate.

4.1. The uniform laterally driven plate

It will be appreciated that only symmetric modes, i.e., modes symmetric with respect to the plate central axis running normal to the plate driven edge, will be excited with the uniform lateral excitation described here. We will expect plate lateral response to rise rapidly as the excitation frequency is caused to approach plate resonance frequencies. It is important, therefore, to begin by establishing resonant frequencies over the frequency range of interest.

Using values of 0.333 and 10,000,000 lbs/in^2, (6.895×10^{10} Pa) for the Poisson ratio and Young's modulus, respectively, and a value of 9.75×10^{-2} lbs/in^3 (2698 kg/m^3) for the density of aluminium, theoretical values for the first and second resonant frequencies of the $12 \times 12 \times 0.0625$ in thick aluminium cantilever plate are found to be 14.56 and 88.74 Hz, respectively. The corresponding experimentally measured resonant frequencies are found to be 14.25 and 86.6 Hz. It will be noted that there is very good agreement between theoretical and experimental first mode frequencies. The second mode frequencies agree to within about 2 percent. This is still fairly good as it is generally accepted that mathematically formulated clamped edge boundary conditions are difficult to achieve experimentally. It will also be appreciated that there will be a node line running across the plate when in second symmetric mode free vibration. The mode shape will therefore be more complicated than that of the first mode and will be more difficult to represent mathematically when conducting free or forced vibration analysis. We recall that a peak-to-peak harmonic excitation amplitude of 0.125 in (0.3175 cm) was used in all experimental tests. In view of the symmetry expected in plate response to uniform lateral base excitation it was decided to characterize this response by measuring, or predicting, peak-to-peak plate response at the mid-point along the plate edge opposite to the driven edge.

In Fig. 5, both theoretically predicted and experimentally measured peak-to-peak response are plotted as a function of excitation frequency in a driving frequency range leading up to the first theoretical resonant frequency. Limitations in the dynamic shaker and associated instrumentation preclude the running of experimental tests at a frequency below about 5 Hz.

It is seen in the figure that there is very good agreement between both sets of results for driving frequencies up to about 12 Hz. Beyond 12 Hz it is seen that the excitation frequency is moving in toward the first plate resonant frequency and both experimental and theoretical response amplitudes begin to rise rapidly. In general one will not be interested in results this close to resonance. In this latter region electronic equipment attached to the plate would almost certainly not be able to function satisfactorily. Furthermore, the theoretical model is based on low amplitude response displacements where plate behaviour is still within the linear range. The actual plate behaviour will become highly nonlinear as one moves in on the resonant frequencies. Recognizing that other researchers may wish to compare data presented here with data computed by means of their theoretical models we have presented driving frequencies and response amplitudes of Fig. 5 in digital form in Table 3.

In Fig. 6 we see theoretically predicted and experimentally measured response behaviour for the same square plate with excitation frequencies lying in a range between the first and second plate resonant frequencies. Both sets of results fall off in amplitude as we move away from the first resonant frequency and begin to rise again as we approach the second resonant frequency. Agreement between the two sets of results in the intervening frequencies could be described as fairly good considering the complicated nature of the problem.

We turn next to a non-square plate, i.e., a 12×15 in aluminium plate of the same thickness, i.e., 0.0625 in. Again, the plate is clamped and driven along a 12 in edge and lateral displacements are measured at the extremity of the plate central axis running normal to the driven edge. Using the same material elastic properties, the first and second resonant frequencies are computed to be 9.286 and 57.39 Hz.

Both theoretically predicted and experimentally measured plate response as a function of driving frequency are presented in Fig. 7 for the non-square plate. Driving frequencies range from approximately 5 Hz to a level just below the first plate resonance. It is seen that there is very good agreement between the two sets of values until we move into the area of resonance. As indicated earlier nonlinearities will begin to manifest themselves as resonance is approached.

In Fig. 8 corresponding response data is presented for the same plate with driving frequencies in the range between the first and second plate resonances. Both theoretical and experimental response curves are seen to fall off as we move away from the first resonance and to begin rising again as we approach the second.

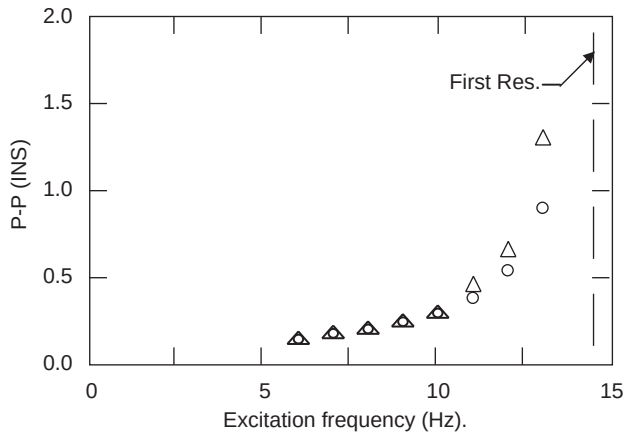

Fig. 5. Theoretical and experimental peak-to-peak lateral response as a function of excitation frequency for square aluminium plate (1 in = 25.4 mm). ○ indicates theoretical values and △ indicates experimental values.

Table 3
Computed numerical values for Peak-to-Peak displacement for $12 \times 12 \times 0.0625$ in. aluminium plate vs. excitation frequency (Hz).

f_f (Hz)	5	6	7	8	9	10	11	12	13
Disp. (in.)	0.151	0.165	0.184	0.210	0.246	0.300	0.387	0.543	0.902

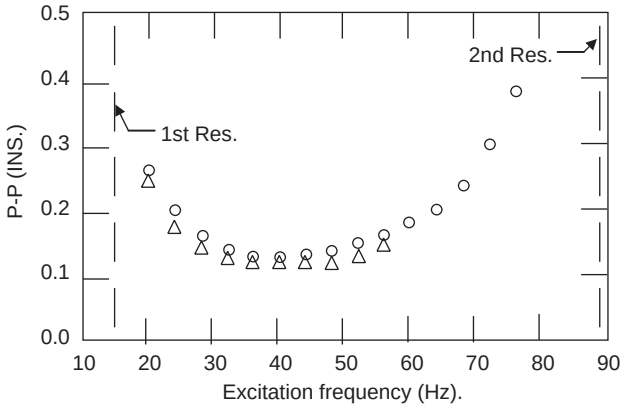

Fig. 6. Theoretical and experimental peak-to-peak lateral response as a function of excitation frequency for square aluminium plate (1 in = 25.4 mm). O indicates theoretical values and Δ indicates experimental values.

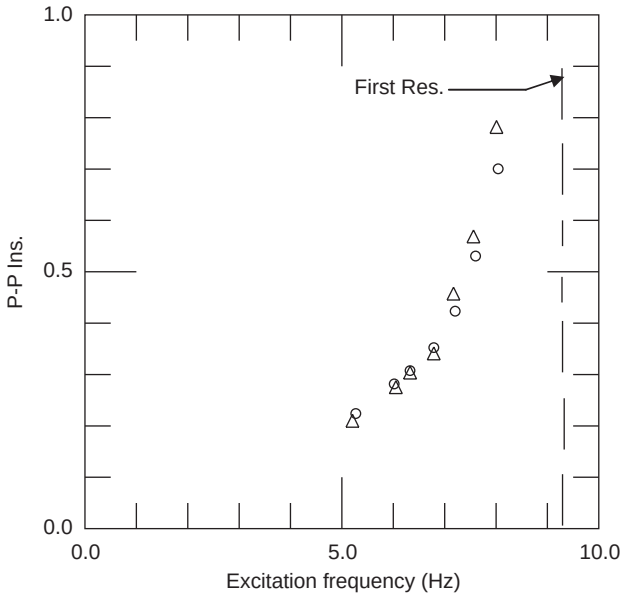

Fig. 7. Theoretical and experimental peak-to-peak lateral response as a function of excitation frequency for 12×15 in aluminium plate (1 in = 25.4 mm). O indicates theoretical values and Δ indicates experimental values.

Agreement between the two sets of values in the region removed from the plate resonances can again be said to be fairly good in view of the complicated nature of the problem. The general character of the two response curves are seen to be almost identical.

4.2. The uniform rotationally driven plate

In this section of the paper we focus attention on a cantilever plate where the clamped base is subjected to a rocking or rotational forced harmonic motion. Experimental data for response of a plate to such excitation was not possible to obtain due to limitations on the shake table and measuring equipment available. Nevertheless, a theoretical study was carried out on the response to be expected from the 12×12 in plate discussed earlier.

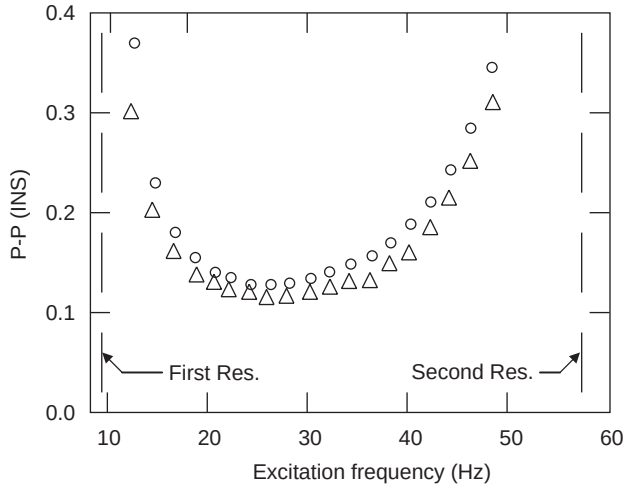

Fig. 8. Theoretical and experimental peak-to-peak lateral response as a function of excitation frequency for 12×15 in aluminium plate (1 in = 25.4 mm). O indicates theoretical values and △ indicates experimental values.

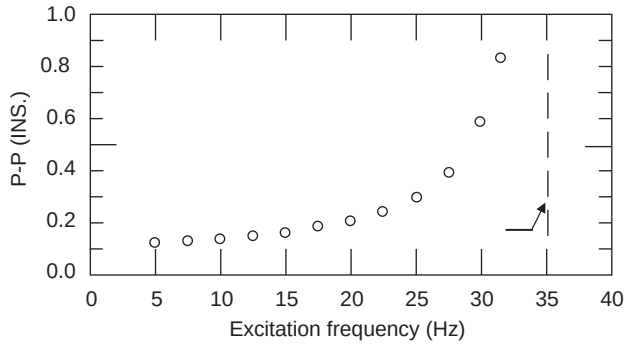

Fig. 9. Theoretical peak-to-peak rotational response as a function of excitation frequency for square aluminium plate (1 in = 25.4 mm). O indicates theoretical values and △ indicates experimental values.

It will be appreciated that the response of a cantilever plate to such excitation must be anti-symmetric about the plate central axis running normal to the driven base. One can characterize the plate response through computation of the plate amplitude of harmonic motion to be expected at the outer corners of the plate, at the extremities of the edge opposite the driven edge. Amplitudes will be identical for each corner. This is the amplitude that is computed and plotted for the theoretical study undertaken here. Amplitudes of response are readily computed utilizing the theoretical model described earlier coupled with Eq. (19).

In Fig. 9 the predicted outer corner peak-to-peak response is plotted as a function of excitation frequency for the 12×12 in plate. Theoretical first and second anti-symmetric mode resonant frequencies, based on plate properties, are found to be 35.16 and 128.5 Hz, respectively. As expected, the computed response begins to rise rapidly as the first resonant frequency is approached. It is particularly clear in this figure that a curve joining the computed points would be projected to approach a value of 0.125 in peak-to-peak amplitude as the driving frequency approaches zero.

In Fig. 10, computed response for the same plate with the driving frequency varying between the first and second resonant frequencies is presented. The fall-off observed in response as we move away from the first resonance and rapid rise as we approach the second is as expected.

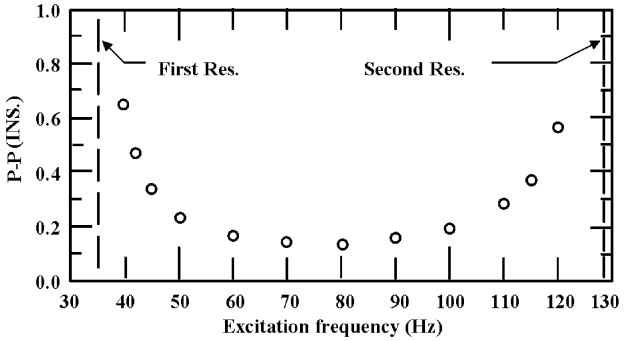

Fig. 10. Theoretical peak-to-peak rotational response as a function of excitation frequency for square aluminium plate (1 in = 25.4 mm). O indicates theoretical values.

5. Discussion and conclusions

It has, over many years, been demonstrated that the superposition method constitutes a powerful mathematical technique for conducting free vibration analysis of rectangular plates. It is demonstrated here, for the first time, that it can also be exploited to obtain accurate analytical type solutions for rectangular plate forced vibration problems. The present work serves, therefore, to open up new doors in the general field of rectangular plate vibration. The problem investigated here involves a cantilever plate subjected to harmonic displacement excitation along its clamped edge. As indicated earlier, the problem is of immediate interest in connection with the projecting of lifetimes of electronic equipment mounted on such plates.

Experimental work reported serves to impart a high degree of confidence in the theoretical model and analytical procedure employed.

It will be apparent, based on earlier free vibration work [4], that there are vast families of other rectangular plate free vibration problems, involving different combinations of boundary conditions, which can be resolved following analytical procedures similar to that described here. This includes plates driven by harmonic point forces acting on plate edges or on plate lateral surfaces. Plate response to harmonic line loading, or forced harmonic line displacements, are well within the realm of capabilities of the analytical procedure described. It is anticipated that numerous problems of the type described are amenable to solution by means of the mathematical modelling approach described here.

Acknowledgements

Experimental work was carried out at the David Florida Laboratory of the Canadian Space Agency in Ottawa, Canada. The authors would like to acknowledge the valuable assistance of Tony Russiello in conducting the experimental tests.

References

[1] Y. Mochida, S. Ilanko, Bounded natural frequencies of completely free rectangular plates, *Journal of Sound and Vibration* 311 (2008) 1–8.
[2] R. Szilard, *Theory and Analysis of Plates*, Prentice-Hall, Englewood Cliffs, NJ, 1974.
[3] D.J. Gorman, Free vibration analysis of cantilever plates by the method of superposition, *Journal of Sound and Vibration* 49 (1976) 453–467.
[4] D.J. Gorman, *Free Vibration Analysis of Rectangular Plates*, Elsevier North-Holland, Inc., New York, 1982.
[5] A.W. Leissa, Free vibration of rectangular plates, *Journal of Sound and Vibration* 31 (1973) 257–293.